Lawrence Berkeley National Laboratory
LBL Publications

Title
Influence of neutron-capture reactions on the nucleosynthesis of strontium

Permalink
https://escholarship.org/uc/item/2n38w8c7

Journal
Communications Physics, 9(1)

ISSN
2399-3650

Authors
Harris, Caley M
Spyrou, Artemis
Denissenkov, Pavel
et al.

Publication Date
2026-06-08

DOI
10.1038/s42005-026-02713-5

Copyright Information
This work is made available under the terms of a Creative Commons Attribution License, available at https://creativecommons.org/licenses/by/4.0/

Peer reviewed

eScholarship.org Powered by the California Digital Library
University of California

communications physics

A Nature Portfolio journal

Article

https://doi.org/10.1038/s42005-026-02713-5

Influence of neutron-capture reactions on the nucleosynthesis of strontium

Check for updates

Caley M. Harris[1,2], Artemis Spyrou[1,2] ✉, Pavel Denissenkov[3], Falk Herwig[3], Andrea L. Richard[1,4], Sivahami Uthayakumaar[1], Dennis Muecher[5], Hannah C. Berg[1,2], Paul DeYoung[6], Alexander C. Dombos[1], Beau Greaves[7], Ann-Cecilie Larsen[8], Sean N. Liddick[1,9], Stephanie M. Lyons[10], Gerald Owens-Fryar[1,2], Alicia Palmisano-Kyle[1,2,11], Georgios Perdikakis[12], Daniel Santiago-Gonzalez[13], Guy Savard[13], Sunniva Siem[8], Mallory K. Smith[1], William W. VonSeeger[6,14] & Mathis Wiedeking[15]

The astrophysical intermediate neutron-capture process (i process) has been reinvoked in recent years to describe stellar observations that cannot be explained by the traditional nucleosynthesis processes. Despite its success, significant uncertainties still remain including the exact astrophysical conditions and site, as well as the nuclear physics input. Available i-process models strongly underproduce the abundance of strontium (Sr) compared to observational data, while successfully describing neighboring elements, like yttrium (Y) and zirconium (Zr). This discrepancy has been attributed to nuclear physics uncertainties, specifically to the unconstrained reaction rate of the neutron-capture on the isotope krypton-88. Here we present an experimental investigation of this reaction and show that our result provides a possible solution to the aforementioned Sr underproduction in i-process models.

The stellar synthesis of elements heavier than iron has been at the forefront of nuclear astrophysics since the 1950s[1,2]. Three processes were established as being responsible for heavy element nucleosynthesis: the slow (s)[3] and rapid (r) neutron-capture processes[4–6] and the p process which is dominated by photodisintegration reactions[7,8]. Starting in the 1990s, however, new astronomical observations have forced the scientific community to reevaluate this picture[9–13] and propose new possible nucleosynthesis processes. Among the proposed new processes, the intermediate (i) process has been successful in, at least partly, reproducing observed abundance patterns[12,14–16].

The i process, as the name implies, corresponds to conditions that lie between those of the s and r processes both in terms of neutron densities ($N_n = 10^{13}$ - 10^{15} n/cm^3) and in terms of time scales (of the order of minutes). Such conditions can be achieved in stellar environments where hydrogen- and helium-induced reactions can occur together, i.e. in a single convection zone. This enhances neutron production via the ^{13}C(α,n)^{16}O reaction because it allows the replenishment of ^{13}C by the ^{12}C(p,γ)^{13}N(e$^+$ν)^{13}C sequence. Different astrophysical sites have been investigated as possible hosts for the i process, such as thermally-pulsing asymptotic giant branch (AGB) and post-AGB stars, as well as in rapidly accreting white dwarfs (RAWDs)[17–25], super-AGB stars[26], the core-He flash in low-mass stars[27] and in massive stars[28]. Depending on the astrophysical assumptions and conditions, elements all the way up to the lead region can be reached if the relevant neutron densities are sustained long enough to achieve sufficiently high neutron exposures[25,29]. The process could even possibly extend into the actinide region under certain conditions, producing Th and U[30,31].

In addition to uncertainties in describing the astrophysical environment, i-process calculations also have significant uncertainties in their nuclear physics input[16,32]. The nuclei involved in i-process models are up to ten neutrons away from the most neutron-rich stable isotope for each element. While most of the nuclear properties, such as masses, half-lives, and β-delayed neutron emission probabilities, are available experimentally, neutron-capture reactions are almost completely unconstrained by

[1]Facility for Rare Isotope Beams, Michigan State University, East Lansing, MI, USA. [2]Department of Physics and Astronomy, Michigan State University, East Lansing, MI, USA. [3]Astronomy Research Centre and Department of Physics & Astronomy, University of Victoria, Victoria, BC, Canada. [4]Department of Physics and Astronomy, Ohio University, Athens, OH, USA. [5]Institute for Nuclear Physics, University of Cologne, Köln, Germany. [6]Department of Physics, Hope College, Holland, MI, USA. [7]Department of Physics, University of Guelph, Guelph, ON, Canada. [8]Department of Physics, University of Oslo, Oslo, Norway. [9]Department of Chemistry, Michigan State University, East Lansing, MI, USA. [10]Pacific Northwest National Laboratory, Richland, WA, USA. [11]Department of Physics and Astronomy, University of Tennessee, Knoxville, TN, USA. [12]Department of Physics, Central Michigan University, Mount Pleasant, MI, USA. [13]Physics Division, Argonne National Laboratory, Argonne, IL, USA. [14]Department of Physics and Astronomy, University of Notre Dame, Notre Dame, IN, USA. [15]Nuclear Science Division, Lawrence Berkeley National Laboratory, Berkeley, CA, USA. ✉e-mail: spyrou@frib.msu.edu

experiments. Out of the hundreds of participating neutron-capture reactions, sensitivity studies have identified a small number that affects the abundance of each of the elements produced in the i process[29,33–35]. These studies are a strong guide for performing impactful experiments, to better characterize i-process conditions and contributions to stellar nucleosynthesis[15,35].

With the successes of i-process models in reproducing at least some of the abundance distributions, we can now look more closely at particular patterns where discrepancies appear and use them to better understand the astrophysical conditions. Here we investigate a puzzle that has been observed since the introduction of the i process when comparing models to elemental abundances in carbon-enhanced metal-poor (CEMP) stars. The amount of Sr in a large fraction of these CEMP star observations seems to be strongly underproduced by the models, while the same models show excellent agreement with the abundances of neighboring elements such as Y and Zr[11,13,14,25,33]. In the present work, we investigate whether this discrepancy can be resolved through more accurate nuclear physics input. Two independent sensitivity studies by Denissenkov et al.[33] and by Martinet et al.[35] have shown that the main reaction impacting the production of Sr within i-process models is the ^{88}Kr(n,γ)^{89}Kr reaction. Here, we focus on experimentally constraining this reaction and exploring its impact on the production of Sr within the i process.

In the absence of experimental data, neutron-capture reaction rates for the i process are calculated using the Hauser-Feshbach statistical model[36]. Within this model the reaction cross section calculation is dominated by three main quantities: the optical model potential (OMP) which describes the interaction between the neutron and the nucleus, the nuclear level density (NLD) which is a measure of the number of available levels per unit energy at a given excitation energy, and the γ-ray strength function (gSF) which describes the γ deexcitation of the nucleus as a function of γ-ray energy for a specific multipolarity and electromagnetic character. For reactions relevant to the i process, the OMP is considered relatively well constrained[37], while different models of NLD and gSF can result in significant variations in the reaction cross section, of the order of 10 or even more. Therefore, when a direct neutron-capture measurement is not possible, indirect techniques often focus on measuring the NLD and gSF for the compound nucleus of interest and in this way constraining the neutron-capture reaction cross section[15,38,39].

In the present work, we report, to the best of our knowledge, on the first experimental constraint of the ^{88}Kr(n,γ)^{89}Kr reaction rate. Due to the short half-life of ^{88}Kr (2.8 h), a direct measurement of this reaction is currently not possible. Instead, we provide a strong experimental constraint by using indirect techniques[40–43], where we populate the compound nucleus of interest, ^{89}Kr, from the β^- decay of ^{89}Br and extract its NLD and gSF. Prior to our measurement, the variation in the theoretical reaction rate was presented in the work of Denissenkov et al.[33] to be roughly a factor of 8.0 using the code TALYS 1.6[44]. In our recent investigation of the neighboring reaction, ^{87}Kr(n,γ)^{88}Kr, we showed that this factor is probably underestimated since it only includes the default predictions of various NLD models and not the parameter variations within each NLD model[43]. The goal of the present work was, therefore, to measure the NLD and gSF of the ^{89}Kr compound nucleus and to extract an experimentally-constrained ^{88}Kr(n,γ)^{89}Kr reaction rate, which can be used in i-process models.

Results and discussion

We performed an experiment to investigate the gSF and NLD in ^{89}Kr and constrain the reaction rate of interest ^{88}Kr(n,γ)^{89}Kr. The experimental details are described in the Methods section. The resulting NLD and gSF were extracted using the β-Oslo method[40,41] and were used as inputs in the calculation of the ^{88}Kr(n,γ)^{89}Kr reaction rate. The calculations were done using the statistical model code TALYS 1.96[44] and the resulting reaction rate is shown in Fig. 1 by the orange band. The light-blue band in the same figure represents the range of theoretical predictions before our measurement, combining the available NLD and gSF models in TALYS, using default parameters. Including parameter variations would make the light-blue band even wider[43]. It can be observed that the overall uncertainty in the reaction cross section is reduced based on the experimental result. In addition, in Fig. 1, the theoretical prediction adopted by the nuclear reaction library REACLIB[45], often used in astrophysical calculations, is shown in the dashed line. The experimentally constrained cross section is systematically lower than the default value, and its overall uncertainty is reduced to approximately a factor of three.

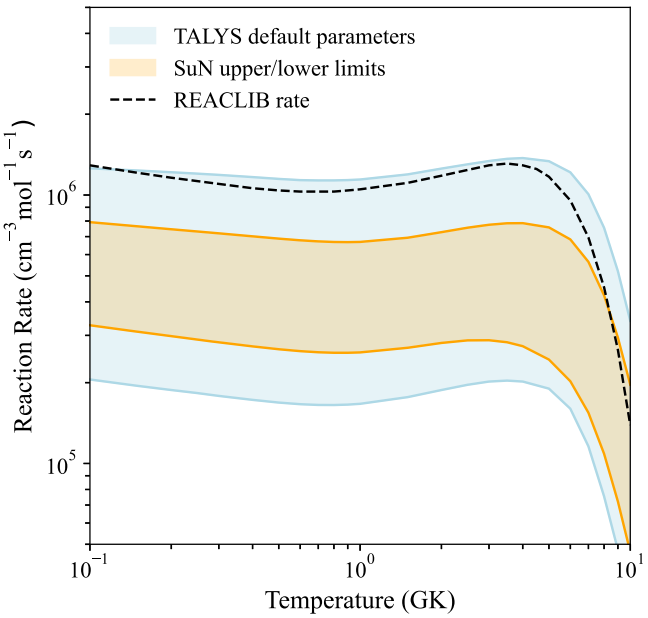


Fig. 1 | Reaction rate of the ^{88}Kr(n,γ)^{89}Kr reaction. The broad light-blue band corresponds to the theoretical calculation of the reaction rate using TALYS 1.96 and combinations of the available NLD and gSF models using default parameters. Including parameter variations would make the light-blue band even wider. The orange band corresponds to the experimentally constrained rate of the present work. The black dashed line represents the recommended rate from the JINA REACLIB library[45].

We investigated the impact of our measurement on the production of Sr in i-process nucleosynthesis calculations using two types of models commonly used in the literature, namely one-zone and multi-zone models. Simple one-zone calculations are typically done with conditions that keep the neutron-density constant[29,33,34]. While the astrophysical conditions are oversimplified in such models (and it is not clear whether such conditions can be realized in multi-zone models), their value lies in isolating the impact of the nuclear physics input for particular neutron densities and investigating if they are viable candidates for the i process. One-zone models do not provide reliable absolute abundances, however they are often used to study ratios of neighboring elements or to investigate the impact of reaction rates. Here we performed one-zone calculations following the prescription of Denissenkov et al. [29,33] using temperature and density values of $T = 2 \times 10^8$ K and $\rho = 10^4$ g/cm^3, and a fixed neutron density of 3.16×1014 n/cm^3, which corresponds to conditions found in RAWD models[33]. In this model, 10,000 Monte Carlo (MC) calculations were done where the reaction rates of 1256 (n,γ) reactions from ^{60}Co to ^{240}Pb were varied within their theoretical uncertainty with a flat probability distribution[33]. The results of these calculations for Sr production are shown in the top panel of Fig. 2. The abundance is presented as the ratio of the resulting abundance from each of the 10,000 MC calculations over the Sr abundance produced when using all default reaction rates, $X_{default}$(Sr). The blue and yellow regions represent MC calculations where the ^{88}Kr(n,γ)^{89}Kr reaction rate was higher and lower than the average rate, respectively. The significant bifurcation observed in this plot is an indication that the Sr production strongly depends on the ^{88}Kr(n,γ)^{89}Kr reaction rate. The bottom panel of Fig. 2 shows the same calculation where the only change was the use of the experimental reaction

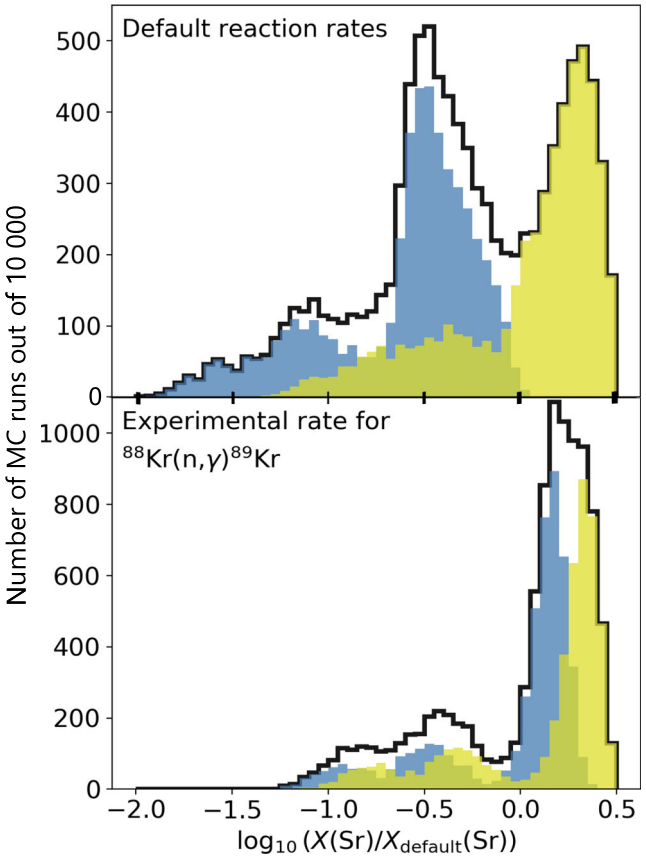


Fig. 2 | Impact on Sr production. Bifurcation plots showing the impact of the present measurement on the Sr abundance. The calculations were done with a fixed neutron density of 3.16 × 1014 n/cm^3 following the prescription of Denissenkov et al.[33]. The top panel shows the Sr abundance, with respect to the default calculation, using the theoretical range of the ^{88}Kr(n,γ)^{89}Kr reaction rate. The bottom plot shows the same calculation when using the experimental reaction rate from the present work. The blue/yellow colors represent the subset of runs where the ^{88}Kr(n,γ)^{89}Kr reaction rate was above/below the default value.

rate from the present work. It is clear that by using our results, the uncertainty in the calculated Sr production is greatly reduced. The remaining tails in the bottom panel are due to the impact of uncertainties in other nuclear reactions.

We further used the one-zone calculations to explore the apparent underproduction of Sr discussed in the introduction, via the [Sr/Y] and [Y/Zr] ratios. These elements are available in observations for a large number of stars and can be used as an important constraint to theoretical calculations. Fig. 3 shows stellar observations from the JINABase[46] for a number of stars marked as CEMP-s or CEMP-i (blue and orange triangles). We include both types of stars since the criteria for their characterization are rather crude, causing overlaps between the various categories. As stated in the JINABase publication[46] the label CEMP-s corresponds to stars with [Ba/Fe]>1.0, [Ba/Eu]>0.5 and [Ba/Pb]>-1.5, while the CEMP-i label includes stars with 0< [La/Eu]<0.6 and [Hf/Ir]~1.0. The colored dots in Fig. 3 connected by the grey dotted line represent model calculations for neutron densities between 10^{12} and $10^{15.5}$ n/cm^3 (color scale shown by the sidebar) using default reaction rates from REACLIB[45]. It can be seen that the default predictions do not agree with most of the available data, and specifically they underproduce the [Sr/Y] ratio. Calculations with the same model, implementing the experimentally-constrained rate of the present work, are shown with the colored star symbols, connected by the solid green line. The new result causes the calculations to shift towards higher values of [Sr/Y] into the region of the figure where the majority of the stellar observations are located. This is true for neutron densities in the range 10^{14}–10^{15} n/cm^3. For lower neutron densities the impact of the new rate is not as significant and at those densities the majority of the observation data points are not reproduced.

To explore further the impact of our measurement we also performed multi-zone i-process nucleosynthesis calculations. These models use more realistic astrophysical conditions and are more appropriate for comparing to the observed i-process abundances of individual elements. Such calculations have been performed for different i-process sites such as RAWDs[23,24] and AGB or post-AGB stars[20–22] with good overall reproduction of observations, although the underproduction of Sr is a common feature. Here we used a multi-zone i-process model based on the convective He-shell structure of the RAWD model G from Denissenkov et al.[24] and incorporating a 100-fold enhanced hydrogen ingestion rate, resulting in a peak neutron density of $N_n^{max} = 10^{15.4}$ n/cm^3. Our calculations suggest that increasing the mass of the RAWD leads to an enhancement of the H-ingestion rate. Therefore, the implemented 100-fold enhanced entrainment rate would represent a RAWD with higher mass. The maximum neutron density achieved in this model is comparable to the value reported by Choplin et al.[47] for their 1 $M_\odot$ AGB model at [Fe/H] = −2.5. Since the neutron density in these models decreases from this maximum value at the base of the He convective zone to much lower values on the order of 10^6 n/cm^3 toward the top, the equivalent neutron density in a one-zone model would be at least an order of magnitude lower than the peak in the multi-zone models.

The results of the multi-zone RAWDs calculation are also shown in Fig. 3 (colored squares). It can be observed that in the multi-zone model the new reaction rate causes the [Sr/Y] ratio to shift towards higher values, but the effect is not as severe as in the one-zone models. This is in line with what was observed in previous studies for the impact of the ^{66}Ni(n,γ)^{67}Ni reaction[34,48]. This is a result of the fact that while multi-zone models include a broad range of neutron densities, the effective (mass-averaged) neutron density is relatively low, much lower than the maximum reported neutron density N_n^{max}. Fig. 3 also shows the time evolution of the abundances, starting at solar values (0,0) and ending at the final values (colored squares). This time evolution corresponds to the reaction network flow over time with the accompanying nuclear burning. It is clear that the impact of the new ^{88}Kr(n,γ)^{89}Kr reaction rate moves the predictions more into the region of stellar observations. Since we don't know the exact time when the He convective zone is split and the i-process is terminated as a result of enhanced H-ingestion rate, the termination could happen anywhere along the dashed lines.

In the present work, we report on the experimental constraint of the ^{88}Kr(n,γ)^{89}Kr reaction rate using the β-Oslo method. This reaction was identified in i-process sensitivity studies as the most impactful reaction for the production of Sr. The new reaction rate is consistently lower than theoretical predictions. The experimentally constrained rate was used in one-zone and multi-zone calculations to investigate its impact on the Sr/Y ratio, which has been systematically underproduced by astrophysical models. With the new rate, all models predict higher production of Sr and are more consistent with the available observations of CEMP stars. The agreement with observations is better at higher neutron-densities in the one-zone model. The impact of the new rate was more moderate on the multi-zone calculation, at least for the full evolution. A higher production of Sr is observed in the multi-zone calculation at earlier times, which corresponds to higher neutron densities as well. These observations indicate that other parameters in the multi-zone models might need to be explored to achieve better agreement with observations or that the i process could be terminated earlier. With the main source of nuclear uncertainty constrained, we recommend further investigation with state-of-the-art astrophysical models to fully understand the discrepancy between models and observations in this mass region.

Methods

Experiment

The experiment was performed at the CARIBU facility at Argonne National Laboratory. An ^{89}Br beam was delivered to the center of the Summing NaI

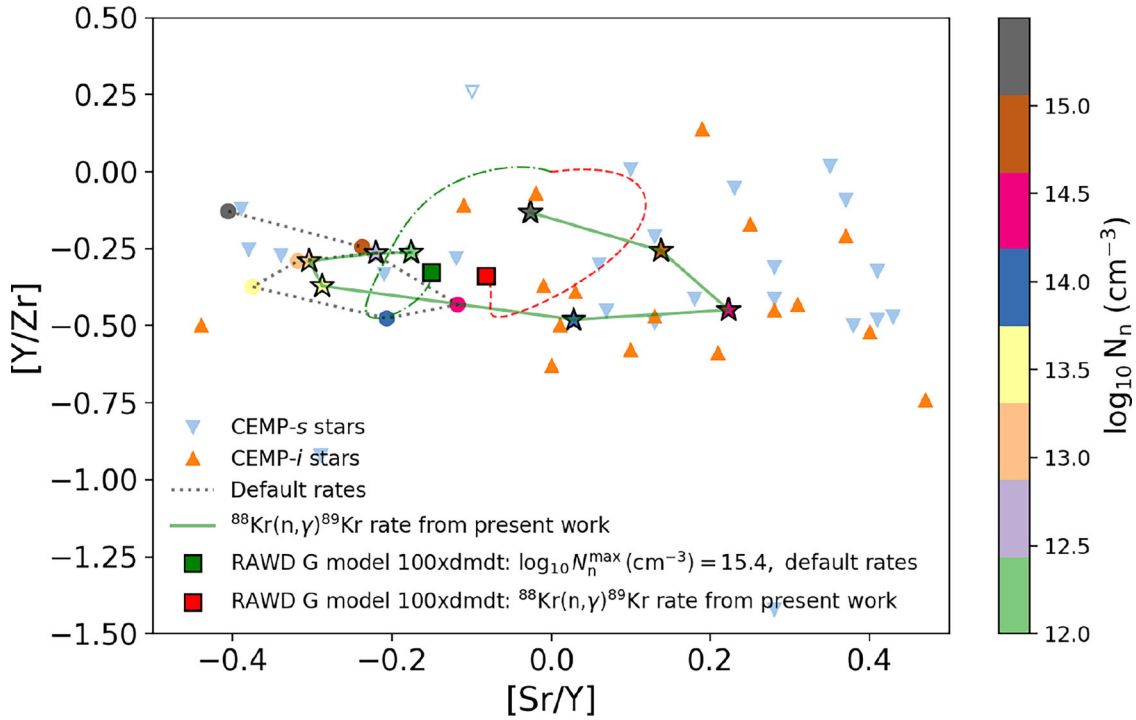


Fig. 3 | Comparison to astronomical observations. Observations of CEMP-s (blue) and CEMP-i (orange) stars from the JINABase[45] showing [Y/Zr] versus [Sr/Y] (in dex). The uncertainties in these observations are of the order of 0.5 dex. The colored dots and star-symbols correspond to one-zone calculations with a fixed neutron density according to the color scale shown. The grey-dotted and green-solid lines connect the colored dots and stars, respectively, to guide the eye. The colored dots correspond to calculations using default reaction rates as presented in Denissenkov et al.[33]. The colored stars are calculations where the only change is the ^{88}Kr(n,γ)^{89}Kr reaction, which was taken from the experimental result of the present work. Colored squares represent the results of multi-zone simulations using default rates (green square) and the value of the ^{88}Kr(n,γ)^{89}Kr reaction rate from the present work (pink square). The green dot-dashed and pink dashed lines show the time evolution of the abundance ratios, starting at solar values (0,0) and ending at the respective colored squares.

(SuN) detector[49], which is a γ-ray total absorption spectrometer developed at Michigan State University. The beam was implanted in the SuNTAN tape transport system[50] in order to remove isobaric contamination. Gamma rays were measured in SuN in coincidence with β particles detected by a plastic scintillator barrel detector (SuNSPOT) that surrounded the implantation point[50]. The barrel detector had 32 wavelength-shifting optical fibers embedded in the plastic, which collected the scintillation light and transported it to two photomultiplier tubes outside of SuN.

SuN consists of eight optically isolated segments, with four above and four below the beam axis. The energy deposited in each segment is sensitive to the individual γ rays (E_γ) emitted from the de-excitation of the produced nucleus, in this case ^{89}Kr. When the energy of each segment is summed event-by-event the total energy deposited in the whole detector is determined, giving information on the populated excitation energy (E_x). A two-dimensional matrix comprised of E_x and E_γ, as shown in Fig. 4, is used as the starting point of this analysis[40,41]. Due to contributions from beam contaminants (isobars) and decay products, two tape cycles were used to isolate the decay of interest ^{89}Br into ^{89}Kr ($T_{1/2}$ (^{89}Br) = 4.3 s). The half lives of the main contaminants are $T_{1/2}$ (^{89}Kr) = 3.1 min and $T_{1/2}$ (^{89}Rb) = 15.4 min. A 20 s beam-on – 20 s beam-off cycle was used to enhance the detection of the ^{89}Br decay, while a 600 s on – 600 s off cycle allowed the identification and subtraction of the child and grandchild contributions.

Analysis

Details of the experimental setup were presented in our previous work[15,43]. The NLD and gSF of ^{89}Kr were extracted using the β-Oslo method[40,41]. This method relies on the assumption that the populated nucleus can be treated statistically, namely exhibits a high enough NLD. This limit was determined by Rauscher et al.[51] to be 10 levels per energy window. For this reason, the present analysis focused on excitation energies above 2.6 MeV as described below.

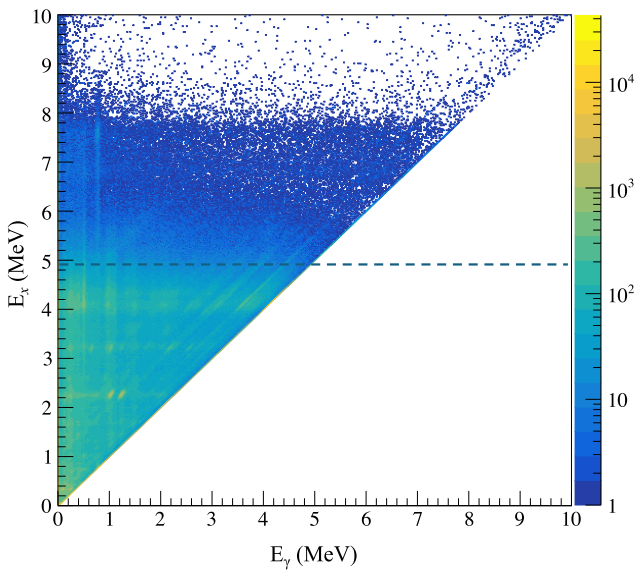


Fig. 4 | Raw experimental data. Raw E_x versus E_γ matrix for the β decay of ^{89}Br into ^{89}Kr. The β-decay Q-value is 8.3 MeV and the neutron-separation energy of ^{89}Kr is 4.9 MeV (dashed line).

The first step in the β-Oslo analysis is to unfold the raw E_x - E_γ matrix (Fig. 4) with the response of the SuN detector[40,52]. The next step is to extract the first-generation γ-ray distribution for each excitation energy bin through an established iterative subtraction process[53]. The produced first-generation matrix can be used to extract the functional form of the NLD and gSF[40,41,54,55].

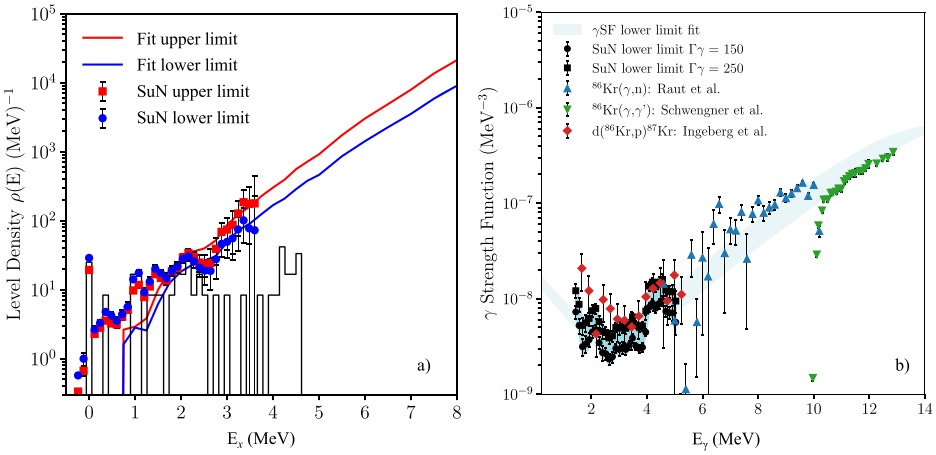


Fig. 5 | Experimental results. a Extracted NLD of ^{89}Kr. The blue and red data points correspond to the upper and lower limits of the present work, while the corresponding lines represent the best fits by adjusting model parameters in the NLD model of Hilaire et al.[61], **b** Extracted gSF of ^{89}Kr (black data points connected by a teal band) showing upper and lower limits in Γ_γ. For comparison, literature values of gSF for neighboring isotopes are also shown[58–60]. The shaded blue area represents the uncertainty of the extracted gSF. In both panels, the vertical lines represent the experimental uncertainties.

Three external normalization parameters need to be used to get the absolute NLD and gSF. Here, we used the energy dependence of the gSF from the neighboring nucleus ^{88}Kr which was measured using the Shape Method[42,43]. Once the slope of the gSF was fixed, the slope of the NLD was also constrained since within the Oslo analysis the two slopes are linked[53]. The absolute scale of the NLD was fit to the discrete levels up to 2.4 MeV, which, according to RIPL-3[56], is the excitation energy up to which the level scheme of ^{89}Kr is considered complete. The final NLD is shown in Fig. 5a. The two variations (upper and lower limit, flat probability distribution) correspond to different assumptions in the analysis such as: the choice of binning, the lower limit in E_γ (1.3-1.6 MeV), and lower accepted excitation energies E_x (2.7–3.6 MeV). It should be noted that the extracted NLD is partial and corresponds to a spin range of 1/2-9/2 of both parities. This range is estimated assuming allowed β^- decays from the ground state of ^{89}Br $(5/2^-)$[57], followed by dipole γ-ray emission. Finally, the absolute scale of the gSF was calculated assuming two limits for the average radiative width, Γ_γ, of 150 and 250 meV used in neighboring nuclei[55,57]. In addition, the analysis limits reported in the NLD were propagated to the gSF. Fig. 5b. shows the lower limit of this analysis in excellent agreement with neighboring Kr isotopes, namely $^{85-87}$Kr[58–60]. The upper limit has a slightly different slope and is higher by approximately a factor of 2, which is still in good agreement with neighboring isotopes since the uncertainties of the relevant experiments are all significant. Both limits were taken into account in the cross section calculation. Overall, uncertainties associated with all steps of the normalization process were taken into account as systematic uncertainties and together with the statistical uncertainties resulted in the overall upper and lower limit shown in Fig. 1 for the reaction rate. The nature of these uncertainties results in a roughly flat probability distribution, which was also used in the astrophysical calculations, as mentioned earlier.

Data availability

The data sets generated during and/or analyzed during the current study are available from the corresponding author on request. Supplementary data, including tables of the NLD, gSF, and Reaction Rate, are publicly available at https://doi.org/10.5281/zenodo.19923921.

Code availability

The codes used for the analysis of the present data are publicly available on GitHub: https://github.com/oslocyclotronlab/oslo-method-software. The astrophysical calculations were performed with codes maintained by the NuGRID collaboration, which are available on GitHub: https://github.com/NuGrid. The theoretical calculations for the reaction rate extraction were performed with the open-source code TALYS: https://nds.iaea.org/talys/

Received: 20 October 2025; Accepted: 28 May 2026;
Published online: 08 June 2026

References

1. Burbidge, E. M., Burbidge, G. R., Fowler, W. A. & Hoyle, F. Synthesis of the elements in stars. *Rev. Mod. Phys.* **29**, 547 (1957).
2. Cameron, A. G. W. Nuclear Reactions in stars and nucleogenesis. *Pub. Astron. Soc. Pac.* **69**, 201 (1957).
3. Kappeler, F., Gallino, R., Bisterzo, R. & Aoki, W. The s process: nuclear Physics, stellar models, and observations. *Rev. Mod. Phys.* **83**, 157 (2011).
4. Arnould, M., Goriely, S. & Takahashi, K. The r-process of stellar nucleosynthesis: astrophysics and nuclear physics achievements and mysteries. *Phys. Rep.* **450**, 97 (2007).
5. Sneden, C., Cowan, J. J. & Gallino, R. Neutron capture elements in the early galaxy. *Ann. Rev. Astr. Ap.* **46**, 241 (2008).
6. Cowan, J. J. et al. Origin of the heaviest elements: the rapid neutron-capture process. *Rev. Mod. Phys.* **93**, 015002 (2021).
7. Arnould, M. & Goriely, S. The p process of stellar nucleosynthesis: astrophysics and nuclear physics status. *Phys. Rep.* **384**, 1 (2003).
8. Rauscher, T. et al. Constraining the astrophysical origin of the p-nuclei through nuclear physics and meteoritic data. *Rep. Prog. Phys.* **76**, 066201 (2013).
9. Bisterzo, S., Gallino, R., Straniero, O., Cristallo, S. & Kappeler, F. The s-process in low-metallicity stars–III. Individual analysis of CEMP-s and CEMP-s/r with asymptotic giant branch models. *MNRAS* **422**, 849 (2012).
10. Dardelet, L. et al. i process and CEMP-s+r stars Proceedings of XIII Nuclei in the Cosmos (NIC XIII). 7-11 July, 2014. Debrecen, Hungary. Online at http://pos.sissa.it/cgi-bin/reader/conf.cgi?confid=204 p. 145. (2014).
11. Hampel, M., Stancliffe, R. J., Lugaro, M. & Meyer, B. S. The intermediate neutron-capture process and carbon-enhanced metal-poor stars. *Astrophys. J.* **831**, 171 (2016).
12. Roederer, I. U., Karakas, A. I., Pignatari, M. & Herwig, F. The diverse origins of neutron-capture elements in the metal-poor star HD 94028: Possible detection of products of i-process nucleosynthesis. *ApJ* **821**, 37 (2016).
13. Hampel, M., Karakas, A. I., Stancliffe, R. J., Meyer, B. S. & Lugaro, M. *Astrophys. J.* **887**, 11 (2019).
14. Herwig, F. et al. Convective-reactive proton-^{12}C combustion in Sakurai's object (V4334 Sagitarii) and implications for the evolution and yields from the first generations of stars. *ApJ* **727**, 89 (2011).
15. Spyrou, A. et al. First Study of the ^{139}Ba(n,γ)^{140}Ba reaction to constrain the conditions for the astrophysical *i* process. *Phys. Rev. Lett.* **132**, 202701 (2024).
16. Wiedeking, M. et al. Unlocking i-process nucleosynthesis by bridging stellar and nuclear physics. *Nat. Rev.* **7**, 696 (2025).

17. Cowan, J. J. & Rose, W. K. Production of 14C and neutrons in red giants. *ApJ* **212**, 149 (1977).
18. Malaney, R. A. Neutron synthesis in AGB and post-AGB stars of low mass. *MNRAS* **223**, 683 (1986).
19. Jorissen, A. & Arnould, M. Proton mixing in He-rich layers - The 13C(alpha,n)16O neutron source and associated nucleosynthesis. *AA* **221**, 161 (1989).
20. Cristallo, S. et al. Asymptotic-giant-branch models at very low metallicity. *Publ. Astron. Soc. Aust.* **26**, 139 (2009).
21. Cristallo, S., Karinkuzhi, D., Goswami, A., Piersanti, L. & Gobrecht, D. Constraints of the Physics of Low-mass AGB Stars from CH and CEMP Stars. *ApJ* **833**, 181 (2016).
22. Karinkuzhi, D. et al. Low-mass low-metallicity AGB stars as an efficient i-process site explaining CEMP-rs stars. *AA* **645**, A61 (2021).
23. Denissenkov, P. et al. i-process nucleosynthesis and mass retention efficiency in He-shell flash evolution of rapidly accreting white dwarfs. *ApJ Lett.* **834**, L10 (2017).
24. Denissenkov, P. et al. The i-process yields of rapidly accreting white dwarfs from multicycle He-shell flash stellar evolution models with mixing parametrizations from 3D hydrodynamics simulations. *MNRAS* **488**, 4258 (2019).
25. Choplin, A., Siess, L. & Goriely, S. The intermediate neutron capture process I. Development of the i-process in low-metallicity low-mass AGB stars. *AA* **648**, A119 (2021).
26. Jones, S. et al. H ingestion into He-burning convection zones in super-AGB stellar models as a potential site for intermediate neutron-density nucleosynthesis. *MNRAS* **455**, 3848 (2015).
27. Campbell, S. W., Lugaro, M. & Karakas, A. I. Evolution and nucleosynthesis of extremely metal-poor and metal-free low- and intermediate-mass stars. II. s-process nucleosynthesis during the core He flash. *AA* **522**, L6 (2010).
28. Banerjee, P., Qian, Y.-Z. & Heger, A. New neutron-capture site in massive Pop III and Pop II stars as a source for heavy elements in the early galaxy. *Ap. J.* **865**, 120 (2018).
29. Denissenkov, P. A., Herwig, F., Perdikakis, G. & Schatz, H. The impact of (n,γ) reaction rate uncertainties of unstable isotopes on the i-process nucleosynthesis of the elements from Ba to W. *MNRAS* **503**, 3913 (2021).
30. Choplin, A., Goriely, S. & Siess, L. Synthesis of thorium and uranium in asymptotic giant branch stars. *AA* **667**, L13 (2022).
31. Vassh, N. et al. Thallium-208: a beacon of in situ neutron capture nucleosynthesis. *Phys. Rev. Lett.* **132**, 052701 (2024).
32. Goriely, S., Siess, L. & Choplin, A. The intermediate neutron capture process II. Nuclear uncertainties. *AA* **654**, A129 (2021).
33. Denissenkov, P. et al. The impact of (n, γ) reaction rate uncertainties of unstable isotopes near N = 50 on the i-process nucleosynthesis in He-shell flash white dwarfs. *J. Phys. G.* **45**, 055203 (2018).
34. McKay, J. E., Denissenkov, P. A., Herwig, F., Perdikakis, G. & Schatz, H. The impact of (n,γ) reaction rate uncertainties on the predicted abundances of I-process elements with $32 \leq Z \leq 48$ in the metal-poor star HD94028. *MNRAS* **491**, 5179 (2020).
35. Martinet, S., Choplin, A., Goriely, S. & Siess, L. The intermediate neutron capture process IV. Impact of nuclear model and parameter uncertainties. *Astron. Astrophys.* **684**, A8 (2024).
36. Hauser, W. & Feshbach, H. The inelastic scattering of neutrons. *Phys. Rev. C.* **87**, 366 (1952).
37. Arnould, M. & Goriely, S. Astronuclear physics: a tale of the atomic nuclei in the sky. *Prog. Part. Nucl. Phys.* **112**, 103766 (2020).
38. Larsen, A. C., Spyrou, A., Liddick, S. N. & Guttormsen, M. Novel techniques for constraining neutron-capture rates relevant for r-process heavy-element nucleosynthesis. *Prog. Part. Nucl. Phys.* **107**, 69 (2019).
39. Spyrou, A. et al. Enhanced production of ^{60}Fe in massive stars. *Nat. Commun.* **15**, 9608 (2024).
40. Spyrou, A. et al. Novel technique for constraining r-process (n,γ) reaction rates. *Phys. Rev. Lett.* **113**, 232502 (2014).
41. Liddick, S. N. et al. Experimental neutron capture rate far from stability. *Phys. Rev. Lett.* **116**, 242502 (2016).
42. Wiedeking, M. et al. Independent normalization for γ-ray strength functions: The shape method. *Phys. Rev. C.* **104**, 014311 (2021).
43. Muecher, D. et al. Extracting model-independent nuclear level densities away from stability. *Phys. Rev. C. Lett.* **107**, L011602 (2023).
44. Koning, A., Hilaire, S. and Duijvestijn, M. C. TALYS: A nuclear reaction program, NRG Report No. 21297/04.62741/P, also available at http://www.talys.eu.
45. Cyburt, R. et al. The JINA REACLIB database: its recent updates and impact on type-I X-ray bursts. *ApJS* **189**, 240 (2010).
46. Abohalima, A. & Frebel, A. JINAbase—a database for chemical abundances of metal-poor stars. *ApJS* **238**, 36 (2018).
47. Choplin, A., Siess, L. & Goriely, A. The intermediate neutron capture process III. The i-process in AGB stars of different masses and metallicities without overshoot. *AA* **667**, A155 (2022).
48. Ingeberg, V. et al. Nuclear level density and γ-ray strength function of ^{67}Ni and the impact on the *i* process. *Phys. Rev. C.* **111**, 015803 (2025).
49. Simon, A. et al. SuN: Summing NaI(Tl)gamma-ray detector for capture reaction measurements. *Nucl. Instr. Meth. Phys. Res. A*. **703**, 16 (2013).
50. Harris, C. et al. SuNTAN: a new tape-transport system for β-decay experiments. *Nucl. Instr. Meth. A*. **1084**, 171185 (2026).
51. Rauscher, T., Thielemann, F.-K. & Kratz, K.-L. Nuclear level density and the determination of thermonuclear rates for astrophysics. *Phys. Rev. C.* **56**, 1613 (1997).
52. Guttormsen, M., Tveter, T. S., Bergholt, L., Ingebretsen, F. & Rekstad, J. The unfolding of continuum γ-ray spectra. *Nucl. Instrum. Meth. Phys. Res. A*. **374**, 371 (1996).
53. Guttormsen, M., Ramsøy, T. & Rekstad, J. The first generation of γ-rays from hot nuclei. *Nucl. Instrum. Meth. Phys. Res. A*. **255**, 518 (1987).
54. Larsen, A. C. et al. Analysis of possible systematic errors in the Oslo method. *Phys. Rev. C.* **83**, 034315 (2011).
55. Schiller, A. et al. Extraction of level density and γ strength function from primary γ spectra. *Nucl. Instrum. Meth. Phys. Res. A*. **447**, 498 (2000).
56. Capote, R. et al. RIPL-reference input parameter library for calculation of nuclear reactions and nuclear data evaluations. *Nucl. Data Sheets* **110**, 3107 (2009).
57. National Nuclear Data Center, Evaluated Nuclear Structure Data File (ENSDF) Retrieval, www.nndc.bnl.gov (2012).
58. Schwengner, R. et al. Pygmy dipole strength in ^{86}Kr and systematics of *N*=50 isotones. *Phys. Rev. C.* **87**, 024306 (2013).
59. Raut, R. et al. Cross-section measurements of the ^{86}Kr(γ,*n*) reaction to Probe the *s*-Process Branching at ^{85}Kr. *Phys. Rev. Lett.* **111**, 112501 (2013).
60. Ingeberg, V. et al. First application of the Oslo method in inverse kinematics. *Eur. Phys. J. A*. **56**, 68 (2020).
61. Hilaire, S., Girod, M., Goriely, S. & Koning, A. J. Temperature-dependent combinatorial level densities with the D1M Gogny force. *Phys. Rev. C.* **86**, 064317 (2012).

Acknowledgements

This research used resources of ANL's ATLAS facility, which is a DOE Office of Science User Facility.

Author contributions

C.M.H. prepared the proposal, prepared and ran the experiment, and performed the analysis of the data. A.S. prepared the proposal, prepared and ran the experiment, supervised the analysis, contributed to the interpretation, and lead the manuscript preparation. P.D. and F.H. identified the reaction, performed the astrophysical calculations, and lead the

interpretation and the results. A.L.R. supported the preparation and execution of the experiment and the analysis of the data. S.U. participated in the data analysis. D.M. supported the data analysis, and in particular the development and implementation of the shape method. P.D.Y. lead the development of the SuNTAN tape system and the SuNSPOT barrel detector and participated in the experiment. S.M.L. developed the proposal, and prepared and ran the experiment. G.P. performed the default TALYS calculations used in the astrophysical model. D.S.G. and G.S. developed and delivered the beam from the CARIBU facility and supported the experiment preparation and execution. W.W.V. supported the experiment preparation through the development of the SuNSPOT detector. H.C.B., A.C.D., B.G., S.N.L., G.O.F., A.P.K. and M.K.S. participated in the experiment preparation and execution, including data taking and online calibrations, and analysis. A.C.L., S.S. and M.W. supported the data analysis and interpretation, in particular the β Oslo and Shape Method components. All authors contributed to the manuscript preparation.

Funding

C.M.H. and A.S. disclose support from the US national Science Foundation (NSF) under Grant No. PHY1913554 and PHY 2209429. A.L.R and S.U. disclose support from the US Department of Energy/National Nuclear Security Administration through the Stewardship Science Academic Alliance (SSAA) under Grant No. DE-NA0003906. D.M. and B.G. disclose support from the Natural Sciences and Engineering Research Council (NSERC) of Canada and the Canada Foundation for Innovation. H.C.B. and G.O.F. disclose support from the Department of Energy/National Nuclear Security Administration through the Nuclear Science and Security Consortium under Award No. DE-NA0003180. P.D.Y. and W.W.V disclose support from the NSF under Grant No. PHY 2209138. W.W.V. also discloses support from the NSF Grant No. PHY2310059. A.C.L. and S.S. disclose support by the Norwegian Nuclear Research Centre under Project No. 341985. A.C.L. also discloses funding from the Research Council of Norway, Grant Project No. 316116. S.N.L. discloses support by the U.S. Department of Energy, Office of Science, Office of Nuclear Physics (DOE-SC-NP), under Contract No. DE-SC-0020451 and DE-SC-0023633. S.M.L. discloses support by the Laboratory Directed Research and Development Program at Pacific Northwest National Laboratory operated by Battelle for the U.S. Department of Energy. D.S.G. and G.S. disclose support by DOE-SC-NP under Contract No. DE-AC02-06CH11357. M.W. discloses support from DOE-SC-NP under Contract No. DE-AC02-05CH11231 as well as from the U.S. Nuclear Data program

Competing interests

The authors declare no competing interests.

Additional information

Supplementary information The online version contains supplementary material available at https://doi.org/10.1038/s42005-026-02713-5.

Correspondence and requests for materials should be addressed to Artemis Spyrou.

Peer review information *Communications Physics* thanks Arthur Choplin and the other anonymous reviewer for their contribution to the peer review of this work. A peer review file is available.

Reprints and permissions information is available at http://www.nature.com/reprints

Publisher's note Springer Nature remains neutral with regard to jurisdictional claims in published maps and institutional affiliations.

Open Access This article is licensed under a Creative Commons Attribution-NonCommercial-NoDerivatives 4.0 International License, which permits any non-commercial use, sharing, distribution and reproduction in any medium or format, as long as you give appropriate credit to the original author(s) and the source, provide a link to the Creative Commons licence, and indicate if you modified the licensed material. You do not have permission under this licence to share adapted material derived from this article or parts of it. The images or other third party material in this article are included in the article's Creative Commons licence, unless indicated otherwise in a credit line to the material. If material is not included in the article's Creative Commons licence and your intended use is not permitted by statutory regulation or exceeds the permitted use, you will need to obtain permission directly from the copyright holder. To view a copy of this licence, visit http://creativecommons.org/licenses/by-nc-nd/4.0/.

© The Author(s) 2026